Eur. Phys. J. E (2015) **38**: 96
DOI 10.1140/epje/i2015-15096-1

THE EUROPEAN PHYSICAL JOURNAL E

Regular Article

A novel method for producing unequal sized droplets in micro- and nanofluidic channels

Ahmad Bedram, Ali Moosavi[a], and Siamak Kazemzadeh Hannani

Department of Mechanical Engineering, Sharif University of Technology, Azadi Ave., P.O. Box 11365-9567 Tehran, Iran

Received 9 April 2015 and Received in final form 24 May 2015
Published online: 11 September 2015 –

Abstract. We propose a novel method for producing unequal sized droplets through breakup of droplets. This method does not have the disadvantages of the available methods and also reduces the dependence of the droplets volume ratio on the inlet velocity of the system by up to 26 percent. The employed method for investigating the proposed system relies on 3D numerical simulation using the VOF algorithm and the results have been obtained with various valve ratios for both the micro- and nanoscale. The results indicate that the droplet length during the breakup process increases linearly with time. The droplet length at the nanoscale is smaller than that at the micro scale. It has been shown that the maximum local capillary number in this system is 2.5 times the average capillary number. Therefore one can use the analytical theories based on the low capillary number assumptions to investigate the method.

1 Introduction

Droplet-based micro- and nanofluidic systems have found various applications in recent years [1,2]. In such systems different processes take place such as droplet transport through porous media [3], droplet motion on the surfaces [4–6], symmetric breakup [7], asymmetric breakup [8,9], stability [10], stratified suspensions [11], generation [12] and transport [13,14]. For example, in the chemical industries we need to transport a corrosive acid. In order to prevent corrosion of the walls of pipes the acid is placed inside a droplet and is transported by a second fluid, namely, the continuous fluid. The droplet does not disperse in the continuous phase [15] and does not have contact with the walls [16] because of the surface tension between two fluids. Also flow circulation inside the droplet increases mixing and homogeneity of the droplet contents [17].

For production of suspensions in the pharmaceutical industries, it can be used from generation of droplets process [18]. The suspensions form by dividing the initial liquids into small droplets.

Over the past decade much research has been conducted on the breakup of an initial droplet into equal sized parts [6,7,19,20], but there has been little research that investigates the breakup of droplets into unequal sized parts in the channels. All the proposed methods for this purpose have some disadvantages that we will explain in the following parts. Then we will introduce a novel method for production of unequal sized droplets that does not have the disadvantages of the available methods.

[a] e-mail: moosavi@sharif.edu

Table 1 shows the comparison of some of the available methods for producing unequal sized droplets by breaking an initial one. Volume ratio (as stated in table 1) is the ratio of the volume of the small generated droplet to the volume of the large generated droplet.

In the method of Choi *et al.* [24], pneumatic valve pressure specifies the volume ratio of the generated droplets. The disadvantage of this method is that the size of the generated droplets cannot be controlled precisely, because the flow pressure affects the valve structure and by change of the structure of the valve, the droplet volume ratio changes.

In the method of Ting *et al.* [25], by heating the fluid in one of the T-junction branches, the viscosity and hydrodynamic resistance of the heated branch reduces and the larger droplet enters this branch. For example Ting *et al.* [25] have stated that for the large capillary numbers, a temperature of about 40 °C is needed for producing droplets with appropriate volume ratios. Such a large temperature limits the applicability of this method especially in the biological applications.

Using the T-junction with valve method [26,27] one can adjust the droplet volume ratio by tuning the valve after manufacturing the system. The disadvantage of this system is that the dependence of the volume ratio to the system inlet velocity is high. But the geometry of this paper decreases this dependence by up to %26.

There are some other methods for producing unequal sized droplets from an initial droplet. Some of these methods do not need a specific geometry such as: droplet breakup in the turbulent flow [28–30], droplet breakup in

Table 1. The comparison of the available methods for producing the unequal sized droplets.

Author	Method	Disadvantage
Link *et al.* [21]	Putting an obstacle in a channel	Small and large generated droplets are together
Link *et al.* [21]	T-junction with unequal length branches	Increases the pressure drop in the small volume ratios
Bedram and Moosavi [22]	T-junction with unequal width branches	Generation of only one volume ratio
Sehgal *et al.* [23]	Droplet motion in a vertical tube	Small and large generated droplets are together
Choi *et al.* [24]	Passing a droplet through a pneumatic valve	Non-precise volume ratio. Also Small and large generated droplets are together
Ting *et al.* [25]	Symmetric T-junction with a heater	Probability of liquids vaporisation in low pressure locations
Bedram *et al.* [26]	T-junction with valve	High dependence of the volume ratio to the system inlet velocity

the simple shear flow [31–33] and droplet breakup by motion of a droplet in a base fluid [34]. Some of these methods need special geometries such as: bringing two droplets to the main channel of a symmetric T-junction with a small time difference [35], T-junction with unequal length branches [36–38], using the two consecutive convergence-divergence symmetric T-junctions [39], droplet motion in the fields with gravity or body forces [40–42] and heat-transfer-based methods [43]. These methods have disadvantages similar to the disadvantages of the previously mentioned methods.

In almost all of the mentioned methods for increasing the speed of droplet generation, we should increase the continuous fluid velocity, however this changes the volume ratio of the generated droplets. This issue is very important especially in the pharmaceutical industries because the changes of the drugs contents may have substantial effects. Therefore a system is required that reduces the dependence of the volume ratio on the continuous fluid velocity.

In this paper a novel method is introduced for generation of unequal sized droplets that does not have the disadvantages of the available methods and also reduces the dependence of the volume ratio on the continuous fluid velocity by up to 26 percent. The important parameters of the system performance (such as droplet length in the breakup process, the contact lengths of the droplet with the walls during the breakup z_1, z_2 (see fig. 1), velocity of channels and pressure drop) are investigated. The employed research method is a 3D numerical simulation for both micro- and nanoscales using the VOF algorithm. Verification of the results are performed by grid independence and by comparing the results to a benchmark [44]. The results show that the droplet length and z_1 and z_2 in the nanoscales are smaller than that in the microscale. For times less than a specific value (t^*), z_1 and z_2 increase with time linearly, and for times greater than t^*, z_1 and z_2 reduce with time. This is because of the existence of two breakup regimes. We have investigated these regimes in detail. The results indicate that the maximum capillary number of this system is 2.5 times the average capillary number. Therefore, the analytical theory with the assumption of low capillary number [45] can be used for this system.

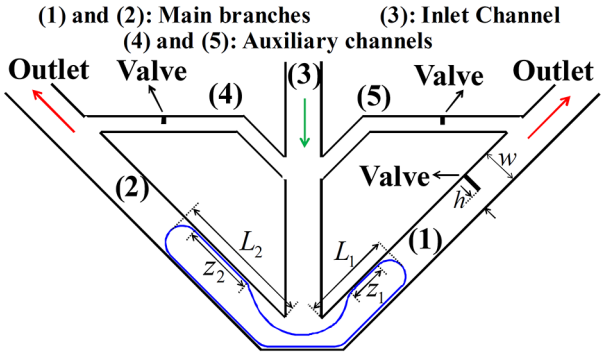

Fig. 1. The geometry of intelligent system and its parameters. The droplet is breaking up into unequal parts.

2 Description of the system

The geometry of the proposed method in this paper is illustrated in fig. 1. We name this system intelligent as it senses the continuous fluid velocity and when this velocity changes, the system adjusts the flow rate of its channels and the changes of the droplet volume ratio become smaller. As can be seen in fig. 1, the intelligent system consists of an inlet channel from which the continuous fluid enters (channel 3) and two branches through which the fluid leaves the system (channels 1 and 2). The auxiliary channels (with the numbers 4 and 5) connect the inlet and branches and, as will be explained, they adjust the system performance. The angle between the inlet channel and the branches, the angle between the inlet channel and auxiliary channels and the angle between the branches and the auxiliary channels were assumed to be 45°. The distance between the system inlet and the beginning of the auxiliary channels is $1w$ and the distance between the system outlets and the end of the auxiliary channels is $1w$, with w as the width of the inlet channel and branches.

The droplet lengths in channels 1 and 2 are shown by L_1 and L_2, respectively. Each of the channels 1, 4 and 5 has a valve for tuning the flow rate in the channels. The valves are in fact adjustable orifice plates and after manufacturing the system one can adjust the degree of opening

of the orifices. Therefore, the adjustable orifice can act as a valve because it can tune the degree of opening of the channel to an arbitrary amount. Application and structure of the adjustable orifice valves have been investigated in a variety of research [46–48].

The initial length of the droplet is long enough to fill the cross section of the branches, that is, until the end of the process, z_1 and z_2 do not diminish.

Some of the parameters used in the analysis are explained as follows: Valve ratio is the ratio of the opening amount of the channel to the channel width ($\lambda = h/w$, h and w are shown in fig. 1). For example, for $\lambda = 1$ the channel is fully open and for $\lambda = 0$ the channel is closed. The volume ratio is the ratio of the small droplet volume to the large droplet volume after breakup ($\tau = V_1/V_2$). The capillary number (the ratio of inertial forces to the surface tension forces) is defined as $Ca = \mu_c U_{in}/\sigma$ where μ_c is the continuous fluid viscosity, σ is the surface tension between two fluids and U_{in} is the inlet velocity of the continuous fluid.

In this paper 3D numerical simulations are performed for both the micro- and nanoscales. The width of the inlet channel and branches are equal and were considered to be 20×10^{-6} m and 100×10^{-9} m for micro- and nanoscales, respectively. The width of the auxiliary channels is assumed to be half of the inlet channel. The cross section of the channels is rectangular and the depth of the channels in the direction that is perpendicular to the sheet is 10 μm and 50 nm for the micro- and nanoscales, respectively.

3 Numerical simulation

For the simulation of the two-phase flow a volume of fluid (VOF) numerical algorithm is applied. The VOF is a surface tracking method for simulation of some immiscible fluids with unknown interfaces. In this method only one equation for the momentum and one equation for the continuity equation are solved. A volume fraction parameter (ϕ) is defined in the domain for each fluid to represent the volume fraction of the fluid in each computational cell. For each computational cell, the physical properties such as density and viscosity are calculated using the volume fraction average of the fluids in the cell.

The flow is assumed to be incompressible and the governing equations are continuity and Navier-Stokes equations as follows:

$$\frac{\partial u_i}{\partial x_i} = 0, \tag{1}$$

$$\rho\left(\frac{\partial u_i}{\partial t} + u_j\frac{\partial u_i}{\partial x_j}\right) = -\frac{\partial P}{\partial x_i} + F_i + \mu\frac{\partial^2 u_i}{\partial x_j^2}, \tag{2}$$

where u_i is the velocity vector in the i direction and ρ and μ are the average density and viscosity of the fluid, respectively. These are derived from the following relations:

$$\rho = \rho_c\phi + \rho_d(1-\phi), \tag{3}$$

$$\mu = \mu_c\phi + \mu_d(1-\phi), \tag{4}$$

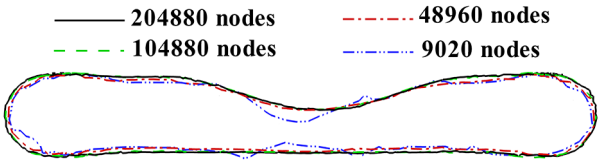

Fig. 2. Checking grid independence of the results.

where the subscripts c and d represent the continuous fluid (that carries the droplets) and the fluids of the droplets, respectively. Also ϕ is the volume fraction of the continuous fluid in each of the computational cells. In each of the computational cells we have $0 \leq \phi \leq 1$. In the VOF model, the interface has a specific thickness because all of the cells that are in the location of the exact interface have $0 < \phi < 1$. So the interface was considered to have positions with $\phi = 0.5$ which were derived by a piecewise linear interface reconstruction method. In this method, the interface is supposed to be linear within the cells that are between the two fluids. Also the advection terms have been calculated using this linear shape [49]. The parameter ϕ was obtained from the following relation:

$$\frac{\partial\phi}{\partial t} + u_i \cdot \frac{\partial\phi}{\partial x_i} = 0. \tag{5}$$

Discretisation of the momentum equation was performed using the second-order upwind and coupling of the pressure and the velocity was conducted by the SIMPLEC algorithm. The convergence is achieved when the residuals R, which are derived from the following relation, become smaller than 0.0007:

$$R_X = \frac{\sum_{P=1}^{N}\left|\sum_{nb} a_{nb}X_{nb} + \Phi - a_P X_P\right|}{\sum_{P=1}^{N} a_P X_P}, \tag{6}$$

where X is a general variable in the cell P, N is the number of all domain cells, nb represents the neighbour cells of the cell P and Φ is the constant part of the source term ($S = S_c + S_P X$) and the boundary conditions.

The boundary condition in the inlet and outlet of the system were considered to be velocity constant and pressure constant, respectively. The densities of the continuous and droplet fluids are 800 kg/m^3 and 1000 kg/m^3, respectively and the viscosities of the continuous and droplet fluids are 0.00125 Pa s and 0.001 Pa s respectively. The surface tension between two fluids is 0.005 N/m.

Grid independence is achieved by solving the droplet breakup problem. Droplet profiles during the breakup process in various grid sizes are given in fig. 2.

As can be seen in fig. 2 for grids with more than 104880 nodes the results are grid independent. In order to ensure grid independence for all the studied cases 448815 nodes were considered.

Bretherton [42] has derived an analytical relation for the velocity of a droplet that transfers through a based fluid flow in a channel as $U = \bar{U}(1 + 1.29(\mu_c U/\sigma)^{2/3})$, where U is the droplet velocity and σ, μ_c and $\bar{U}$ are surface tension between two fluids, viscosity and average velocity

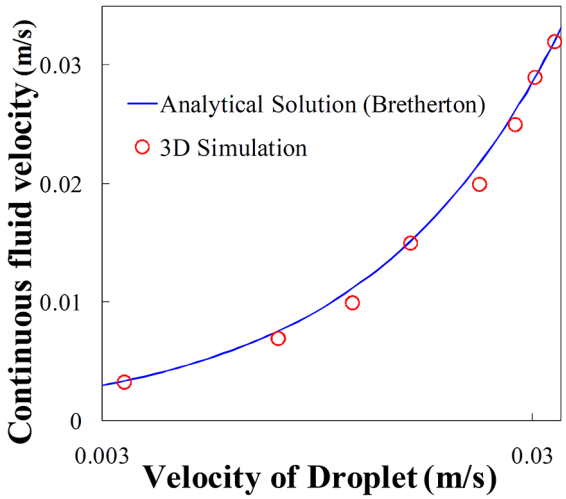

Fig. 3. Comparison of the analytical relation of Bretherton's results [42] with the 3D numerical results of the present study.

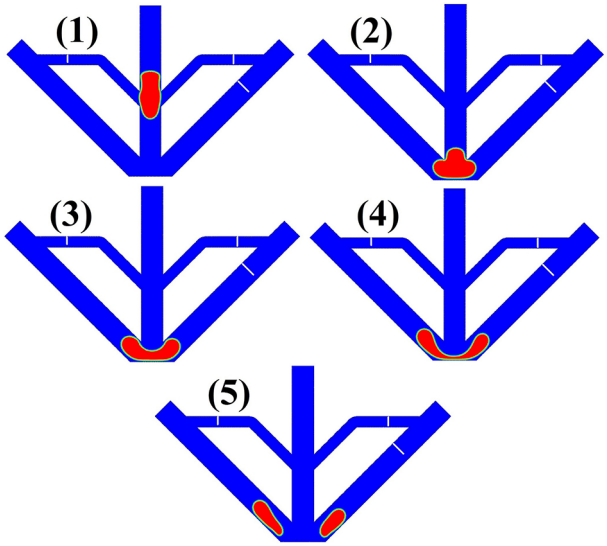

Fig. 4. Droplet breakup process in the intelligent system. By controlling the valves, the channel diameter and the angles between the channels, a vast performance range can be considered for the system.

of continuous fluid, respectively. For verification of our 3D numerical results, we simulated Bretherton's problem and compared our numerical results with Bretherton's analytical relation (fig. 3). As can be seen, very good agreement exists.

4 The system performance

Figure 4 illustrates a sample of droplet breakup process in the intelligent system. When the droplet is in the inlet channel and approaches the auxiliary channels it does not enter them because their width and the flow rate of the continuous fluid are small. When the droplet reaches the center of the junction it deforms and the upper surface of it becomes circular and its thickness becomes low until it

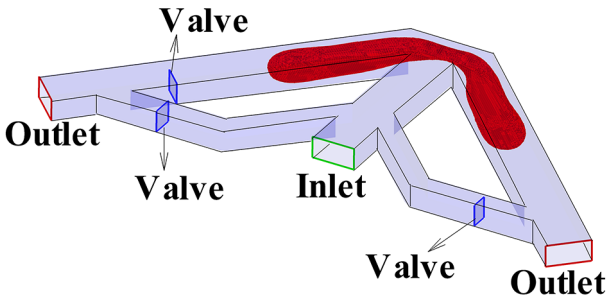

Fig. 5. The droplet deformation at the center of the intelligent system. Two auxiliary channels connect the beginning of the inlet channel to the end of the branches.

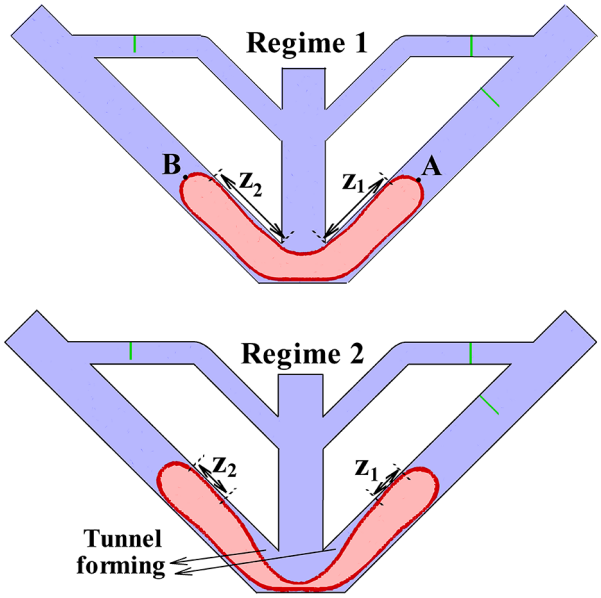

Fig. 6. The two regimes of the droplet deformation during the breakup process. At times less than t^* the droplet is in the first regime.

breaks up into two unequal parts and each part enters one of the branches.

Figure 5 shows a 3D representation of the droplet breakup process in the proposed intelligent system. As can be seen, the droplet is deforming at the center of the junction.

One of the important parameters of the system performance is the droplet length during the breakup process $L_{\text{whole}} = L_1 + L_2$. Droplet length during the breakup has a length equal to L_{whole} as depicted in fig. 1. If this length is reduced we can use smaller tube length for the branches and through reduction of the branch lengths the pressure drop of the system decreases and also the manufacturing cost of the system reduces.

There are two different regimes during the breakup process. In the first regime the continuous fluid that exists on the top of the upper surface of the droplet does not enter the branches and the droplet closes the branch cross section entirely (fig. 6). In this regime the two tips of the droplet that exist in the branches (points A and B

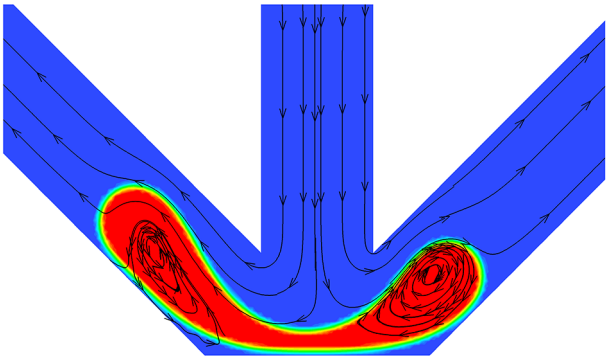

Fig. 7. Large vortexes inside the droplet during the breakup process. As can be seen, the tunnel is formed between the wall and the upper surface of the droplet. To make the illustration clearer, only the center of the junction has been depicted.

in fig. 6) move together in the direction of the continuous fluid flow. In the second regime the continuous fluid enters the branches and the upper surface of the droplet separates from the wall in each of the branches and the continuous fluid flows between the upper surface of the droplet and the wall (fig. 6).

In various applications it is necessary that the mixing of the droplet inside increases. In these applications the valve ratio should reduce such that z_1 reaches zero and the tunnel forms. By tunnel formation, large vortexes form inside the droplet (fig. 7).

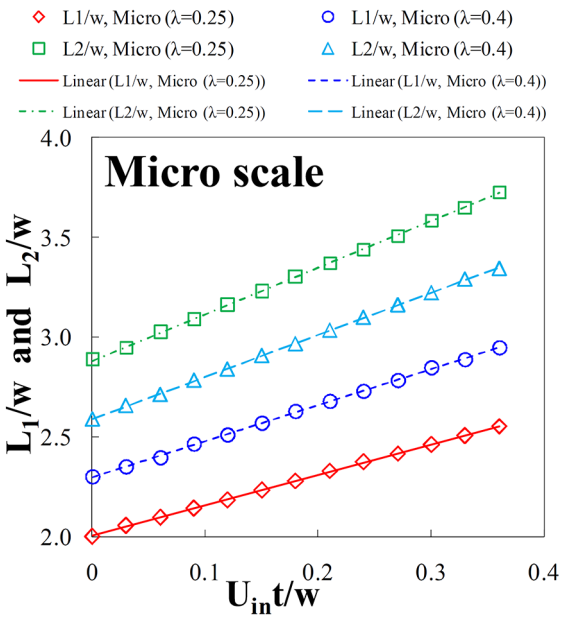

Fig. 8. Droplet length in the channel 1 (L_1) and channel 2 (L_2) as a function of time in the valve ratios 0.4 and 0.25 in the microscale. The droplet length becomes dimensionless using the channel width (w) and the time becomes dimensionless using the inlet velocity (U_{in}) and the channel width. The slope of the curves for the cases L_1 ($\lambda = 0.4$), L_1 ($\lambda = 0.25$), L_2 ($\lambda = 0.4$) and L_2 ($\lambda = 0.25$) are 1.808, 1.526, 2.108, 2.334, respectively.

5 Results and discussion

Figures 8, 9 and 10 illustrate the droplet length in channel 1 (L_1), droplet length in channel 2 (L_2) and the whole length of the droplet during the breakup process for the valve ratios 0.25 and 0.4 and for the micro- and nanoscales. In all of the simulations of the study, the initial time ($t = 0$) is a moment in which the droplet is in a state that is shown in fig. 9. As can be seen, for all cases the droplet length in channel 1 and 2 and the whole length of the droplet increase linearly with the time. In all cases L_2 is larger than L_1 at the initial time because before the droplets arrive at the center of the junction, the flow rate of channel 2 is larger than channel 1 and therefore when the droplet reaches the center of the junction L_2 is larger than L_1. Therefore according to the definition of L_{whole} which is "$L_1 + L_2$", L_{whole} is not equal to zero at the initial time. Considering that the droplet volume is constant during the breakup process as the droplet length in channel 1 becomes larger the droplet length in the channel 2 becomes smaller. As depicted in figs. 8 and 9 for the case micro $\lambda = 0.4$ with the maximum L_1 it has the minimum L_2 and for the case nano $\lambda = 0.25$ with the minimum L_1 it has the maximum L_2.

In the industrial application of the unequal droplet generator systems it is required that the droplet length during the breakup process becomes as small as possible in order to reduce the pressure drop and the manufacturing cost of the system. The results reveal that in the system proposed in this study, L_1 (L_2) in the nanoscale is smaller (larger) than the microscale but the whole length of the droplet during the breakup in the nanoscale is smaller than that in the microscale (see fig. 10). For example, for the case $\lambda = 0.4$ and dimensionless time 0.36 the whole length of the droplet at the nanoscale is 14% smaller than that in the microscale. The results also show that the valve ratio does not affect the droplet length (fig. 10). Thus, for reduction of the droplet length we can use the system in a nanoscale (unlike the microscale).

The results indicate that at both the micro- and nanoscales and for any valve ratio, the increase in rate of L_2 is larger than the increase in rate of L_1. This is due to the fact that the continuous fluid velocity in channel 1 is smaller than channel 2. According to figs. 9 and 10 with the reduction of the valve ratio, L_1 decreases and L_2 increases because by decreasing the valve ratio the volume of the droplet that enters channel 1 reduces and then L_1 decreases and the volume of the droplet that enters channel 2 increases and then L_2 increases. L_1 reduction and increase of L_2 cancel each other and the whole length of the droplet remains constant by the change of the valve ratio. With the decrease of the valve ratio the velocity of the continuous fluid that enters channel 1 decreases and then the slope of the L_1 curve *versus* time reduces. For this reason it can be seen in figs. 8 and 9 that the slope of L_1 curve for the case $\lambda = 0.25$ is smaller than the case $\lambda = 0.4$.

The parameters z_1 and z_2, illustrated in the fig. 1 have an important effect on tunnel forming during the breakup

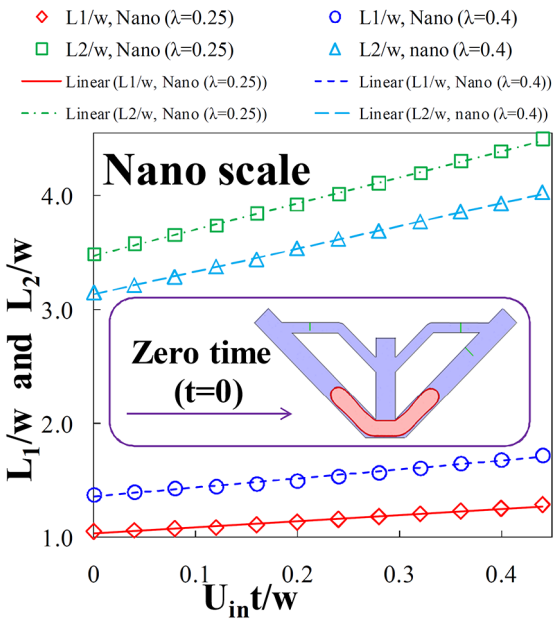

Fig. 9. Droplet length in the channel 2 (L_2) as a function of the dimensionless time for the valve ratios 0.4 and 0.25 and in the micro- and nanoscales. The slope of the curves for the cases L_1 ($\lambda = 0.4$), L_1 ($\lambda = 0.25$), L_2 ($\lambda = 0.4$) and L_2 ($\lambda = 0.25$) are 0.796, 0.537, 2.003 and 2.282, respectively.

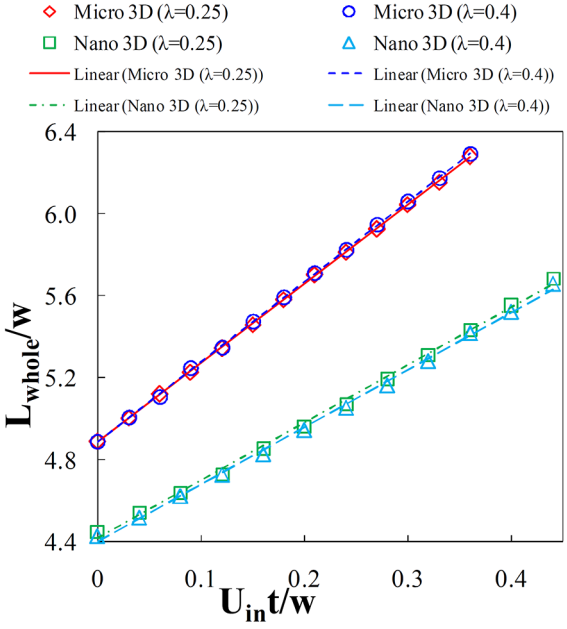

Fig. 10. Whole length of the droplet (L_{whole}) as a function of the dimensionless time in the valve ratios 0.4 and 0.25 and in the micro- and nanoscales. The slope of the curves for the cases micro $\lambda = 0.4$, micro $\lambda = 0.25$, nano $\lambda = 0.4$ and nano $\lambda = 0.25$ are 1.958, 1.930, 1.400 and 1.410, respectively.

process. If during the breakup process z_1 or z_2 reach zero the tunnel forms. Tunnel formation has an important role in some applications (*e.g.* the applications based on the mixing of the droplet inside). For this reason the investigation of z_1 and z_2 variation during the breakup process is an important issue.

Figures 11 and 12 illustrate z_1 and z_2 as a function of dimensionless time in the valve ratios 0.4 and 0.25 and in the micro- and nanoscales. z_1 and z_2 are scaled by the channel width (w) and the time is made dimensionless using the inlet velocity (U_{in}) and the channel width. As can be seen, with respect to time, z_1 and z_2 have two linear and power law function. For the dimensionless time less than 0.12 and 0.16 for the micro- and nanoscale respectively, z_1 and z_2 increase linearly with time. In order to simplify the presentation we refer to the dimensionless time 0.12 and 0.16 for the micro- and nanoscale, respectively, as t^* in the following sections. For the times greater than t^*, z_1 and z_2 decrease with time in terms of a power law function because there are two different regimes during the breakup process.

In the first regime (times less than t^*) the two tips of the droplet that exist in the branches (points A and B in fig. 6) move together in the direction of the continuous fluid flow. Therefore, z_1 and z_2 increase linearly. In the second regime (times more than t^*), over time, more continuous fluid enters the branches and z_1 and z_2 reduce. As illustrated in figs. 11 and 12 by decreasing the valve ratio, a less continuous fluid enters branch 1, z_1 reduces and a more continuous fluid enters branch 2 and, as a result, z_2 increases. Also the results indicate that z_1 and z_2 in the nanoscale are significantly smaller than in the microscale. For example, for the microscale case of $\lambda = 0.25$ and the dimensionless time 0.12, z_1 in the nanoscale is about half of that in the microscale. Thus, for applications in which high mixing is needed, using the nanoscale is more efficient.

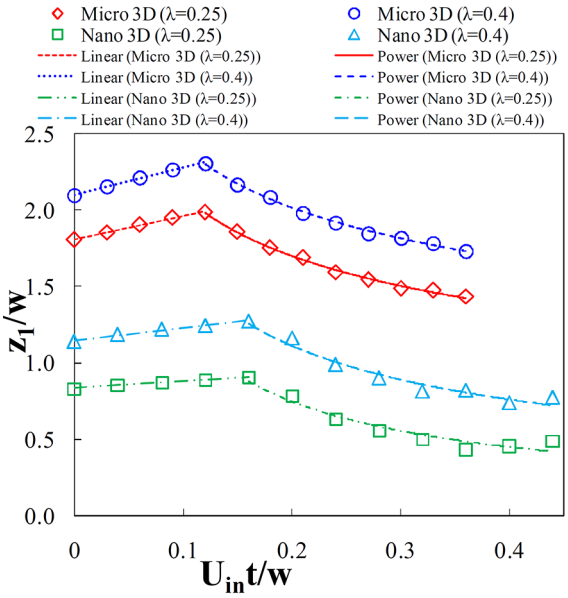

Fig. 11. z_1 as a function of time. The curves can be expressed in terms of a power law function of z_1 for the cases $\lambda = 0.4$ (micro), $\lambda = 0.25$ (micro), $\lambda = 0.4$ (nano) and $\lambda = 0.25$ (nano) as $(z_1/w) = 1.327(U_{\text{in}}t/w)^{-0.25}$, $(z_1/w) = 1.045(U_{\text{in}}t/w)^{-0.3}$, $(z_1/w) = 0.461(U_{\text{in}}t/w)^{-0.54}$ and $(z_1/w) = 0.231(U_{\text{in}}t/w)^{-0.72}$, respectively.

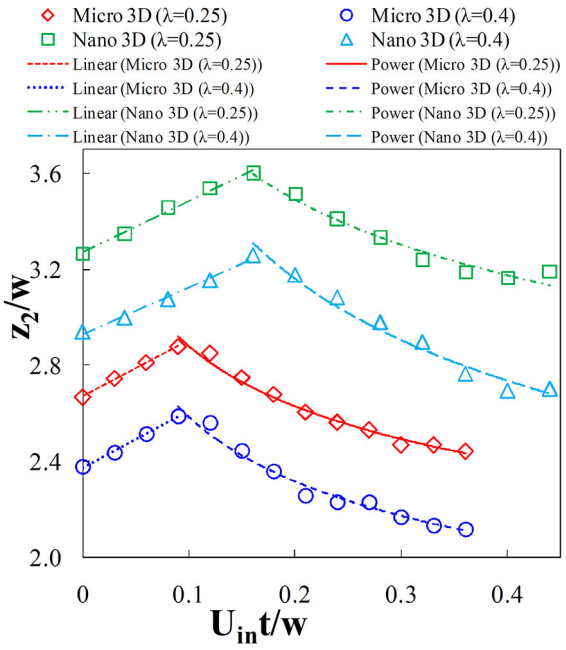

Fig. 12. z_2 as a function of the dimensionless time in the valve ratios 0.4 and 0.25 in the micro- and nanoscales. The power law of z_2 for the cases $\lambda = 0.4$ (micro), $\lambda = 0.25$ (micro), $\lambda = 0.4$ (nano) and $\lambda = 0.25$ (nano) are $(z_1/w) = 1.796(U_{\text{in}}t/w)^{-0.15}$, $(z_1/w) = 2.13(U_{\text{in}}t/w)^{-0.13}$, $(z_1/w) = 2.266(U_{\text{in}}t/w)^{-0.2}$ and $(z_1/w) = 2.804(U_{\text{in}}t/w)^{-0.13}$, respectively.

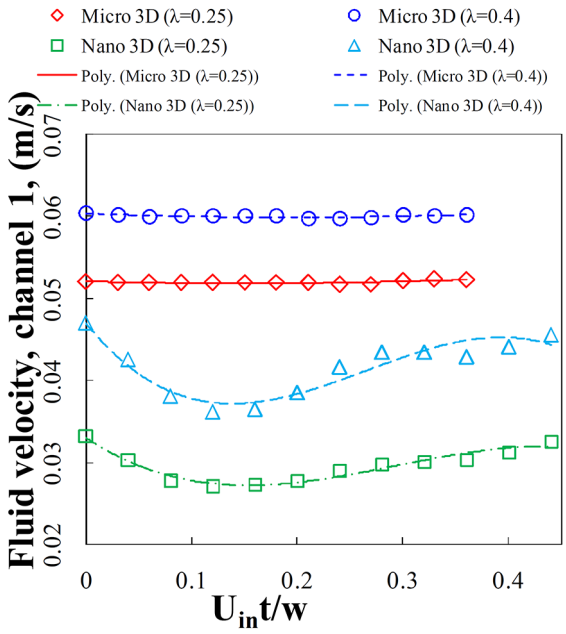

Fig. 13. Continuous fluid velocity of channel 1 as a function of the dimensionless time for $\lambda = 0.4$ and $\lambda = 0.25$ for both the micro- and nanoscales. Micro- and nanoscale curves have been represented by second- and third-order polynomials, respectively.

Figures 13, 14 and 15 represent the continuous fluid velocity of channels 1, 2 and 4, respectively, as a function of time for the valve ratios 0.4 and 0.25 and at the

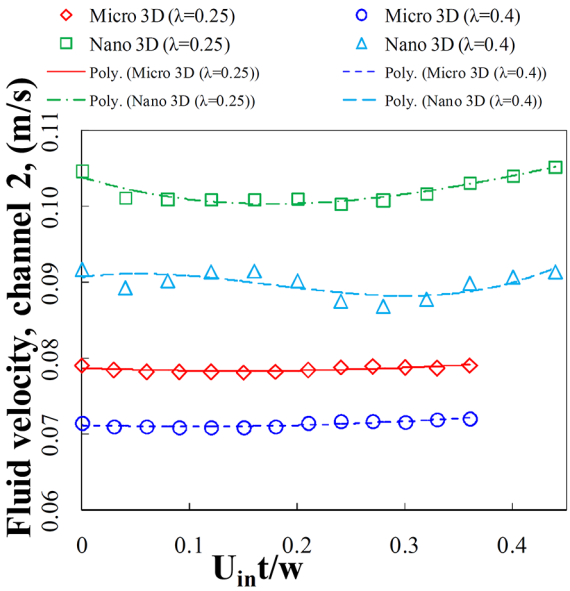

Fig. 14. Continuous fluid velocity of channel 2 as a function of the dimensionless time for $\lambda = 0.4$ and $\lambda = 0.25$ in the micro- and nanoscales. Micro- and nanoscale curves are fitted using second- and third-order polynomials, respectively.

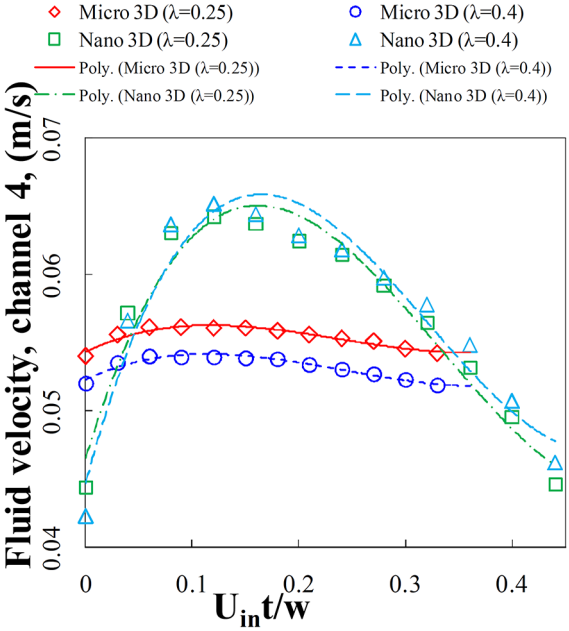

Fig. 15. Velocity of channel 4 as a function of the dimensionless time for $\lambda = 0.4$ and $\lambda = 0.25$ and in the micro- and nanoscales. All of the curves are expressed by third-order polynomials.

micro- and nanoscales. Although the velocity of channels 1 and 2 are not constant with respect to time, their variations are very low. For example for the microscale case and $\lambda = 0.4$ and $\lambda = 0.25$ the ratio of the difference between the maximum and minimum velocity of channels 1 and 2 to the time average velocity is less than 1%. Also for the nanoscale for both $\lambda = 0.4$ and $\lambda = 0.25$ the ratio of the

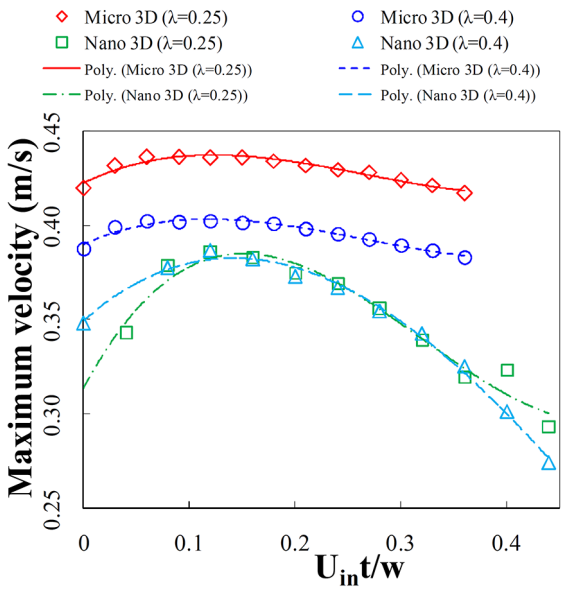

Fig. 16. The maximum fluid velocity of the system as a function of the dimensionless time in the $\lambda = 0.4$ and $\lambda = 0.25$ and in the micro- and nanoscales. All of the curves are expressed using third order polynomials.

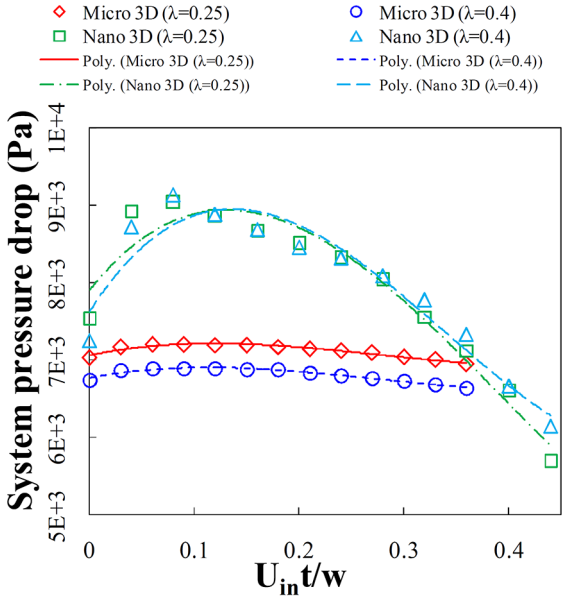

Fig. 17. The system pressure drop as a function of the dimensionless time for $\lambda = 0.4$ and $\lambda = 0.25$ and in the micro- and nanoscales. All of the curves are represented via third-order polynomials. The pressure drop in the nanoscale is scaled by a factor of 0.04.

difference between the maximum and minimum of channel 2 (channel 1) velocity to the time average value is less than 3.5% (14%). With reduction of the valve ratio the hydrodynamic resistance of the channel 1 increases and the velocity of channel 1 reduces and the velocity of channel 2 increases. This issue has been illustrated in figs. 13 and 14.

Figure 15 illustrates that the velocity of channel 4 increases (decreases) with time for the dimensionless times less (more) than t^* (as stated before, t^* is 0.16 for the nanoscale and 0.12 for the microscale) because the droplet breakup process has two different regimes before and after t^* (fig. 6). The results also indicate that the velocity of channel 4 has a low dependence on the valve ratio. For example at the dimensionless time 0.12, difference of the channel 4 velocity between valve ratios 0.4 and 0.25 are less than 4% (2%) for the micro (nano) scale.

Analytical theories that perform for equal and unequal droplet generator systems usually have low capillary number assumption [42,44,45]. So for the method in this paper we present the maximum fluid velocity of the system to find if it is possible to use the analytical theories in this method. Figure 16 shows the maximum fluid velocity of the system for the valve ratios 0.4 and 0.25 in the micro- and nanoscales. As can be seen the maximum fluid velocity in the nanoscale is less than the microscale. Also the maximum velocity of the system increases over time and in the dimensionless time t^* reaches its maximum and after t^* reduces. Therefore the maximum fluid velocity of the system occurs in the dimensionless time t^*. For this research the capillary number (based on the inlet velocity of the system) is 0.04. By consideration of the maximum fluid velocity of the system according to the fig. 16, the maximum locally capillary number of the system for microscale $\lambda = 0.25$, microscale $\lambda = 0.4$ and nanoscale are 0.109, 0.101, 0.0967, respectively. Therefore, the maximum local capillary number of the system is about 2.5 times the average capillary number. Thus, one can use the analytical theories based on the low capillary number assumptions for the present method.

Figure 17 represents the system pressure drop over time in valve ratio 0.4 and 0.25 and in the micro- and nanoscales. As can be seen the pressure drop increases with time and reaches its maximum and then reduces. The maximum pressure drop over time occurs at the dimensionless time t^*. The results show that the pressure drop has a low dependence on the valve ratio. Also the pressure drop in the nanoscale is more than that in the microscale because the diameter of the channels in the nanoscale is smaller than in the microscale.

6 Conclusion

In this study a novel method was proposed for generation of unequal sized droplets. In the suggested method the operation of the system can be adjusted simply after manufacturing it (unlike the available methods). Also this method reduces the changes of the volume ratio due to the valve ratio change by up to 26 percent. To investigate the system we used a 3D numerical algorithm and presented the results for both the micro- and nanoscales. The numerical results were compared with the available analytical results and very good agreement was observed. We investigated the droplet length parameters (L_1, L_2 and L_{whole}) that were important in the reduction of the pressure drop and the system manufacturing cost. The results showed that for all the cases the droplet length (L_1, L_2 and

L_{whole}) increases linearly with the time. Also the droplet length during the breakup process in the nanoscale is less than the microscale. The contact lengths, namely, parameters z_1 and z_2 which have an important role in the applications based on the inside droplet mixing were investigated. It was found that the z_1 and z_2 increase linearly for the dimensionless time less than t^* and decrease in terms of a power law for the dimensionless time more than t^* because there are two different regimes before and after the t^*. We investigated these regimes in details.

Also the results indicated that z_1 and z_2 in the nanoscale are much smaller than those in the microscale and for applications in which high mixing is needed the use of the nanoscale is very useful. The velocity of the system in the channels was investigated and it was found that the dependence of the velocity with time in channels 1 and 2 is very low. It was shown that the velocity of channel 4 has a low dependence on the valve ratio and for times less than t^* (regime 1) increases with the time and for times more than t^* (regime 2) reduces. We investigated the maximum velocity of the system and showed that the maximum local capillary number of the system is 2.5 times the average capillary number. Thus, the analytical theories with low-capillary-number assumptions can be used to study the system. The pressure drop of the system was investigated and it was found that the pressure drop dependence on the valve ratio is small and its maximum occurs at t^*.

References

1. E.A.G. Jamie, R.P.A. Dullens, D.G.A.L. Aarts, J. Phys.: Condens. Matter **24**, 284120 (2012).
2. A. Moosavi, M. Rauscher, S. Dietrich, J. Phys.: Condens. Matter **21**, 464120 (2009) (Special issue).
3. L. Bacri, F.B. Wyart, Eur. Phys. J. E **3**, 87 (2000).
4. S. Moulinet, D. Bartolo, Eur. Phys. J. E **24**, 251 (2007).
5. Z. Yao, M.J. Bowick, Eur. Phys. J. E **34**, 32 (2011).
6. Y.S. Shin, H.C. Lim, Eur. Phys. J. E **34**, 74 (2014).
7. D.A. Hoang, L.M. Portela, C.R. Kleijn, M.T. Kreutzer, V.V. Steijn, J. Fluid Mech. **717**, R4 (2013).
8. T. Fu, Y. Ma, H.Z. Li, AIChE J. **60**, 1920 (2014).
9. J. Wang, D. Yu, *Microfluidics and Nanofluidics*, Accepted Paper, DOI: 10.1007/s10404-014-1458-z, (2014).
10. S.E. Mhatre, S.D. Deshmukh, R.M. Thaokar, Eur. Phys. J. E **35**, 39 (2012).
11. S. Harada, T. Mitsui, K. Sato, Eur. Phys. J. E **35**, 1 (2012).
12. S.H. Tan, S.M. Sohel Murshed, N.T. Nguyen, T.N. Wong, L. Yobas, J. Phys. D: Appl. Phys. **41**, 165501 (2008).
13. J.H. Chang, J.J. Pak, J. Adhes. Sci. Technol. **26**, 2105 (2012).
14. B. Han, H. Meng, J. Power Sources **217**, 268 (2012).
15. H. Liu, Y. Zhang, J. Appl. Phys. **106**, 034906 (2009).
16. G.F. Christopher, N.N. Noharuddin, J.A. Taylor, L.A. Shelley, Phys. Rev. E **78**, 036317 (2008).
17. J. Tice, H. Song, A. Lyon, R. Ismagilov, Langmuir **19**, 9127 (2003).
18. A.K. Kulshreshtha, N. Onkar Singh, G. Michael Wall, *Pharmaceutical Suspensions: From Formulation Development to Manufacturing* (Springer Science & Business Media, 2009) Section 1.2.2.
19. A. Bedram, A. Moosavi, J. Appl. Fluid Mech. **6**, 81 (2013).
20. S. Afkhami, A.M. Leshansky, Y. Renardy, Phys. Fluids **23**, 022002 (2011).
21. D.R. Link, S.L. Anna, D.A. Weitz, H.A. Stone, Phys. Rev. Lett. **92**, 054503 (2004).
22. A. Bedram, A. Moosavi, Eur. Phys. J. E **34**, 78 (2011).
23. B.R. Sehgal, R.R. Nourgaliev, T.N. Dinh, Progr. Nucl. Energy **34**, 471 (1999).
24. J.H. Choi, S.K. Lee, J.M. Lim, S.M. Yang, G.R. Yi, Lab Chip **10**, 456 (2010).
25. T.H. Ting, Y.F. Yap, N.T. Nguyen, T.N. Wong, J.C.K. Chai, L. Yobas, Appl. Phys. Lett. **89**, 234101 (2006).
26. A. Bedram, A.E. Darabi, A. Moosavi, S. Kazemzade, ASME J. Fluids Eng. **137**, 031202 (2014).
27. A. Bedram, A. Moosavi, S. Kazemzadeh, Phys. Rev. E **91**, 053012 (2015).
28. R. Maniero, O. Masbernat, E. Climent, F. Risso, Int. J. Multiphase Flow **42**, 1 (2012).
29. T. Lemenand, P. Dupont, D.D. Valle, H. Peerhossaini, Chem. Engin. Res. Design **91**, 2587 (2013).
30. F. Ravelet, C. Colin, F. Risso, Phys. Fluids **23**, 103301 (2011).
31. F. Abbassi-Sourki, B. Mosto, M.A. Huneault, Rheol. Acta **51**, 111 (2012).
32. Y.K. Wei, Y. Qian, H. Xu, Comput. Multiphase Flows **4**, 111 (2012).
33. M. Desse, J. Mitchell, B. Wolf, T. Budtova, Food Hydrocoll. **25**, 495 (2011).
34. M.S. Korlie, A. Mukherjee, B.G. Nita, J.G. Stevens, A.D. Trubatch, P. Yecko, J. Phys.: Condens. Matter **20**, 204143 (2008).
35. G.F. Christopher, J. Bergstein, N.B. End, M. Poon, C. Nguyen, S.L. Anna, Lab Chip **9**, 1102 (2009).
36. J. Nie, R.T. Kennedy, Anal. Chem. **82**, 7852 (2010).
37. W. Engl, M. Roche, A. Colin, P. Panizza, A. Ajdari, Phys. Rev. Lett. **95**, 208304 (2005).
38. I. Lee, Y. Yoo, Z. Cheng, H.K. Jeong, Adv. Funct. Mater. **18**, 4014 (2008).
39. W. Yining, F. Taotao, C. Zhu, Y. Lu, Y. Ma, H.Z. Li, Microfluid Nanofluid **13**, 723 (2012).
40. V. Cristini, J. Blawzdziewicz, M. Loewenberg, Phys. Fluids **10**, 1781 (1998).
41. H.N. Yoshikawa, F. Zoueshtiagh, H. Caps, P. Kurowski, P. Petitjeans, Eur. Phys. J. E **31**, 191 (2010).
42. A.J. Griggs, A.Z. Zinchenko, R.H. Davis, Int. J. Multiphase Flow **34**, 408 (2008).
43. Y.F. Yap, S.H. Tan, N.T. Nguyen, S.M. Sohel Murshed, T.N. Wong, L. Yobas, J. Phys. D: Appl. Phys. **42**, 065503 (2009).
44. F.P. Bretherton, J. Fluid Mech. **166**, 10 (1961).
45. A.M. Leshansky, L.M. Pismen, Phys. Fluids **21**, 023303 (2009).
46. J.D. Crounse, K.A. McKinney, A.J. Kwan, P.O. Wennberg, Anal. Chem. **78**, 6726 (2006).
47. N. Wongprasert, M.D. Symans, ASCE J. Structural Eng. **131**, 867 (2005).
48. S.S. Parmar, S.W. Benson, J. Phys. Chem. **92**, 2652 (1988).
49. D.L. Youngs, Numer. Methods Fluid Dyn. **24**, 273 (1982).